IEEE Access
Multidisciplinary | Rapid Review | Open Access Journal

Received December 14, 2018, accepted January 8, 2019, date of publication January 23, 2019, date of current version February 12, 2019.

*Digital Object Identifier 10.1109/ACCESS.2019.2894393*

# Design of Low-Cost Personal Identification System That Uses Combined Palm Vein and Palmprint Biometric Features

**PENG CHEN, BAOJIN DING, HAIXIA WANG, RONGHUA LIANG, (Senior Member, IEEE), YILONG ZHANG, WEI ZHU, AND YIPENG LIU**

College of Information and Engineering, Zhejiang University of Technology, Hangzhou 310023, China

Corresponding author: Yipeng Liu (liuyipeng@zjut.edu.cn)

This work was supported in part by the Natural Science Foundation of China under Grant 61527808 and Grant 61602414, and in part by the Hangzhou Major Science and Technology Innovation Project under Grant 20172011A027.

**ABSTRACT** This paper proposes a low-cost personal identification system that uses the combined palm vein and palmprint biometric features. The system consists of near-infrared and visible light-emitting diode (LED) arrays, a low-cost visual sensor, a Xilinx chip, and other components. A real-time image quality assessment (IQA) method for the combined palm vein and palmprint biometric features is also proposed. Two types of the LED with central frequency spectra of 890 and 680 nm are used to capture the palm vein and palmprint, respectively. The adaptive feedback control of the diode brightness is in accordance with the image quality assessed by the combined 2D entropy and local 2D entropy. The palm vein and palmprint images are acquired nearly simultaneously, and each acquired image undergoes a few preprocessing steps for extraction of the vein and print patterns. We use an image-level wavelet-based fusion strategy to reduce image storage requirement for the embedded platform and implement a complex wavelet-based fusion strategy for the PC platform. A deep scattering convolutional network is applied for extracting the features of the fused images, and a multi-class support vector machine is used for training and recognition. Characteristics of some vision-based personal identification systems are discussed. The proposed real-time IQA method with fusion strategy and feature extraction algorithm in our prototype system has substantially less operational requirements than that of the previous fusion strategies. It also demands less memory and yields lower equal error rate than the classical feature extraction algorithms.

**INDEX TERMS** Biometrics, low-level image analysis, feature extraction and description, image circuits and architectures, hardware/software co-design.

## I. INTRODUCTION

Compared with traditional personal identification methods, which are based on token or knowledge, biometric technologies are gaining popularity because their unique features are difficult to forge [1]. Biometric features, such as fingerprint [2], palmprint [3], iris [4], [5], face [6], [7], and vein [8], are highly reliable. Similar to fingerprints and palmprints [9], [10], vein patterns do not change with age. A vein pattern is a network structure of blood vessels underneath the human skin. It effectively protects against possible external damages, spoof attacks, and impersonation [11]. This pattern is nearly invisible to the naked eye under visible light (VL) but can be acquired under near-infrared (NIR) illumination. Vein patterns have many types, including palm [12], palm dorsal [13], finger [14], wrist [15], forearm [16], and scleral veins [17]. Biometric recognition using palm vein characteristics is emerging as a touchless and spoof-resistant method of identifying individuals or verifying their identities [18], thereby attracting widespread attention. Meanwhile, instead of the use of palm vein alone, the fusion of palm vein and palmprint is regarded as a reliable means of accurately determining the identity of an individual [19], [20].

The low quality of a vein image seriously affects the recognition rate. Thus, the characteristics of visual sensors are considered in NIR vein acquisition system design. The finger vein images captured by dynamic luminance were introduced in the literature [21]. Crisan *et al.* [22] focused on improving the two essential components of vein-scanning devices,

namely, hardware lighting systems and feature extraction algorithms. In palmprint and palm vein processing, instead of the entire image, only a region of interest (ROI) is used for recognition. ROI extraction considerably affects the quality of palm vein features. Lee [23] described an ROI extraction algorithm that is based on two points of the palm. Many verification algorithms using biometric features of hand veins have been developed over the past decade. Wang *et al*. [24] employed the Hausdorff distance to generate matching scores between extracted line patterns and obtained promising results. Principal component analysis (PCA) and Fisher linear discriminant (FLD) analysis are classical algorithms adopted for data representation and compression. 2DPCA and 2DFLD were developed by Yang *et al.* [25] and Xiong *et al.* [26], respectively. Mutelo *et al.* [27] proposed a novel feature extraction algorithm in face recognition using 2DPCA along with 2DFLD. In the recognition domain, such as face recognition, these 2D methods are based on 2D image matrices rather than 1D vectors. Thus, the image does not need to be transformed into a vector prior to feature extraction [27]. 2D methods demand lower overall computational complexity and perform better than 1D methods. However, features extracted by these methods are not translation- or rotation-invariant. Deep convolutional networks provide state-of-the-art classification and regression results over many high-dimensional problems [28], such as image classification with thousands of complex classes [29] and speech recognition [30]. Bruna and Mallat [31], [32] proposed a scattering network with predefined filters and architectures. Minaee and Wang [33] used a deep scattering convolutional network (DSCN) for fingerprint recognition.

Researchers usually utilize expensive visual sensors that cost approximately US$1,000 to US$10,000, such as Lynx-2048-GigE [34] and GL2048R [35], to achieve excellent image quality. However, using these sensors in daily life is extremely costly. Thus, the present study introduces a low-cost combined palm vein and palmprint personal identification system (LPVPPIS), which comprises a self-designed mainboard, a low-cost visual sensor, an array of NIR light-emitting diodes (LEDs) and VL LEDs, and a boost converter driver circuit. The main contributions of this work are as follows.

1) We demonstrate, for the first time, an energy-efficient LPVPPIS that can achieve comparatively higher recognition rate with substantially less operation requirement and less memory requirement than state-of-the-art methods.

2) A real-time image quality assessment (IQA) method based on 2D entropy and local 2D entropy is proposed for the acquisition of palm images with improved quality.

The remainder of the paper is organized as follows. Section 2 presents the system development. Section 3 illustrates the preprocessing steps, the IQA method, and an image-level fusion strategy. Section 4 presents the feature extraction and recognition algorithms. Section 5 demonstrates the database creation and experimental results. Section 6 provides the discussion, and conclusions are drawn in Section 7.

## II. SYSTEM DEVELOPMENT

### A. INTEGRATED SYSTEM DEVELOPMENT

As shown in Fig. 1, the proposed LPVPPIS is built on a self-designed main board and an LED board. The main board is based on a Xilinx Zynq-7020 SoC [36] that integrates a process system with dual ARM cortex-A9 processors and a hardware programmable logic (PL) with a field-programmable gate array (FPGA). Two different types of LED with central frequency spectra at 890 and 680 nm are designed and integrated into the LED board to capture the palm vein and palmprint simultaneously. The images are acquired by a low-cost complementary metal-oxide-semiconductor transistor (CMOS) camera and controlled by the PL in the SoC with an LED driving circuit. Thus, the palm vein and palmprint images can be captured, shown on the display, and saved on an SD card simultaneously. In our proposed system, only one camera is used to capture the palm vein and palmprint images, and the two images are obtained nearly simultaneously. Thus, image fusion can be performed without additional errors caused by calibration, unlike with a two-camera system similar to that in the literature [37].

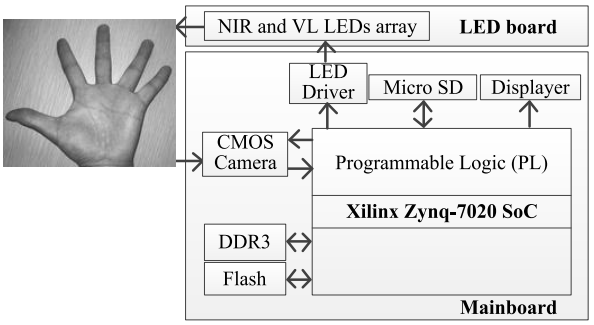


**FIGURE 1.** Architecture of the proposed system.

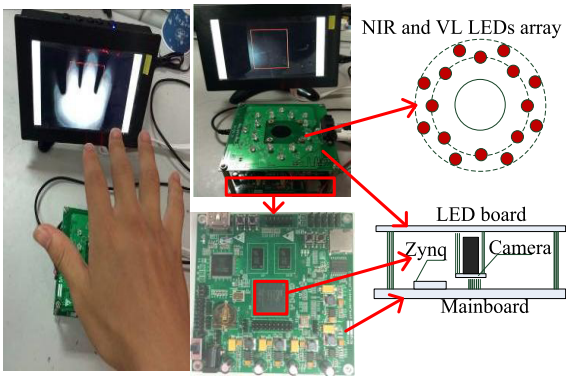


**FIGURE 2.** Integrated system developed for LPVPPIS.

The overall acquisition system on the printed circuit board (PCB) shown in Fig. 2 is small and compact with a size of approximately 100 mm × 100 mm. The users simply need to position their hands freely above the prototype to capture.

The OV2640 [38] CMOS camera is connected to the PL through general-purpose input/output ports in the main board and captures the images. The LED board has a boost converter MP3202 [39], which drives the LED array from a 5 V DC voltage. The MP3202 uses the constant current, which is measured by an external current sense resistor, to drive the LEDs.

### B. SOFTWARE SCHEME FOR PROPOSED SYSTEM

Figure 3 illustrates the proposed LPVPPIS software scheme, where two different types of LED are switched to capture the palmprint and palm vein images. Each image acquired undergoes a few steps of image preprocessing for extraction of the vein and print patterns, as shown in Section 3.1. An IQA method is proposed for adaptively controlling the LED brightness in accordance with feedback, and details are provided in Sections 3.2 and 3.3. We use an image-level fusion strategy to reduce the image storage requirement and the following feature extraction operations for the embedded platform. Thereafter, a small database that contains the fused palm vein and palmprint images is created. The feature extraction algorithm is developed using a DSCN, and a multi-class support vector machine (SVM) is used for training and recognition. Details are discussed in Section 4.

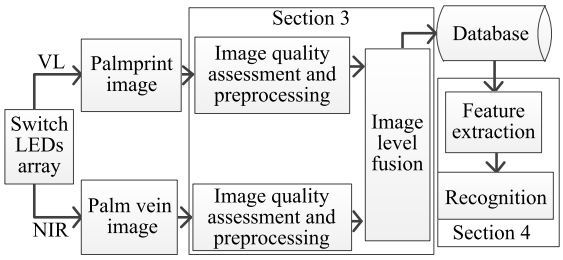


**FIGURE 3.** Scheme of the proposed LPVPPIS.

## III. IMAGE PREPROCESSING, QUALITY ASSESSMENT, AND FUSION STRATEGY

### A. PREPROCESSING

The preprocessing of palm vein and palmprint images consists of several steps, including binarization, rotation, ROI extraction, denoising, and enhancement, as shown in Fig. 4. The preprocessing of a palm vein image is similar to that of a palmprint. The Otsu algorithm [40] is used to perform the binarization. Figure 4 shows the results, where the background is black, and the palm region is white. Hand contour is extracted from the palm images, where the valley points P1 (between the valley point of the pinky and ring fingers) and P2 (between the valley point of the middle and index fingers) are selected as the reference points. The palm image is then rotated to be vertical. A rectangular region with length-to-width ratio of 1.2 is cut from the palm image as the ROI using the key points P1 and P2 as the top left and top right corners, respectively. A size normalization algorithm is implemented through linear interpolation to ensure that the ROI region of different vein images has the same size. Wavelet thresholding

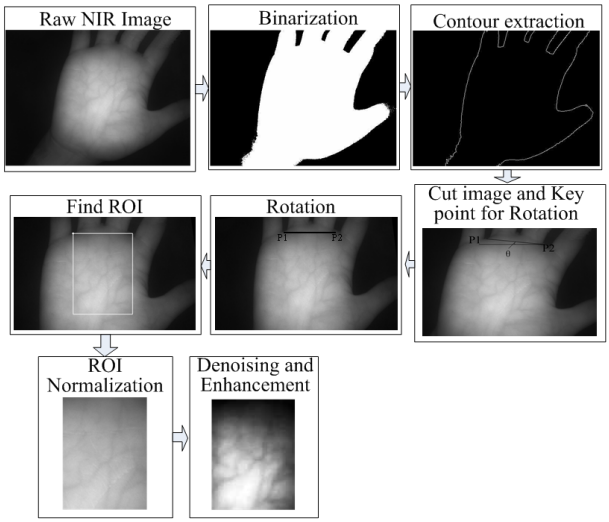


**FIGURE 4.** Preprocessing of palm images.

and histogram equalization are performed on the ROI image to remove the noise and enhance the image for further feature extraction.

### B. IMAGE QUALITY ASSESSMENT (IQA) BASED ON 2D ENTROPY AND LOCAL 2D ENTROPY

Image quality is highly dependent on illumination intensity because of the characteristic of spectroscopy technology for palm image capture. Improved quality of raw images leads to enhanced recognition performance of the proposed system. A pulse width modulation (PWM) controller is generated by a control unit of the image acquisition subsystem constructed as a hardware module in the PL for controlling the illumination of the LED array. The PWM signal controller is connected to the internal duty cycle register and the period register inside the PL. Thus, the different operating cycles output to the external LED drive circuit directly.

The NIR and VL intensity is controlled by the PWM duty cycle in the range of 5% to 50% with 15% step. The results of the palm vein images at different levels of NIR illumination intensity are shown in Fig. 5. The image shown in Fig. 5 (c) is more suitable for personal identification than that in Fig. 5 (d), which is overexposed and does not clearly show the features of the vein. Duty cycle, environment lighting, and human hand conditions can affect the image quality. Thus, an automatic environment-adaptive duty cycle setting is required for maintaining excellent image quality.

IQA methods are normally applied for evaluating a distorted image given availability of the original image [41]. By contrast, our IQA method is used for evaluating the palm image acquired in our system without the original image. A non-reference-based IQA method is proposed for estimating the image quality using 2D entropy and local 2D entropy.

The 2D entropy-based IQA method can estimate image quality and adjust the duty cycle automatically. The 2D entropy can evaluate the signal-to-noise ratio. Thus, it is used

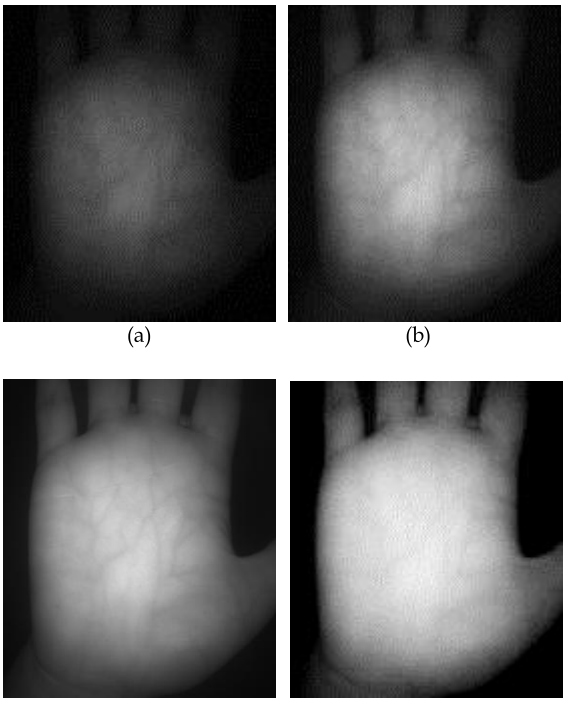


**FIGURE 5.** Palm vein images at different levels of infrared illumination intensity. (a) PWM duty cycle: 5%. (b) PWM duty cycle: 20%. (c) PWM duty cycle: 35%. (d) PWM duty cycle: 50%.

for quality assessment as follows:

$$H_{2D}(P) = \frac{1}{m \times n} \sum_{i=0}^{255} \sum_{j=0}^{255} L_{ij} \log_2(\frac{m \times n}{L_{ij}}), \tag{1}$$

where $m$ and $n$ are the image height and width, respectively; $i = f(x, y)$ is the gray value of the pixel at coordinate $(x, y)$, $0 \leq x < m$, $0 \leq y < n$; $j = g(x, y)$ is the average gray value of the neighboring pixels around $(x, y)$, as calculated as follows:

$$g(x, y) = \frac{1}{D \times D} \sum_{\Delta x=-\frac{D-1}{2}}^{\frac{D-1}{2}} \sum_{\Delta y=-\frac{D-1}{2}}^{\frac{D-1}{2}} f(x + \Delta x, y + \Delta y), \tag{2}$$

where $D$ is the window size, $L_{ij}$ is the frequency of the pixel pair $(i, j)$, and $L_{ij}$ can be calculated from the statistical distribution of the histogram. The image resolution from the OV2640 is 1600×1200 pixels. Thus, $m = 1600$, $n = 1200$. The information required in our system is primarily in the ROI of the palm. Thus, a local 2D entropy is also proposed as follows:

$$H_{2D\_Local}(P) = \frac{1}{s \times t} \sum_{i=0}^{255} \sum_{j=0}^{255} L_{ij} \log_2(\frac{s \times t}{L_{ij}}), \tag{3}$$

where $s$ and $t$ are the ROI image height and width, respectively. The quality of the acquired images is then assessed by the 2D image entropy and the local 2D entropy. The brightness of the LED array can be controlled on the basis of the feedback image quality and then recaptured until a high-quality pattern image is achieved.

The PL resource are used to calculate the 2D entropy and local 2D entropy in real time. The resource utilization and running time of 2D entropy and local 2D entropy program are show in Tables 1 and 2, respectively.

**TABLE 1.** PL resource utilization and running time of 2D entropy program.

| Step | Clock | DSP48E | FF | LUT | RT(ms) |
|---|---|---|---|---|---|
| I | 150M | 99 | 7591 | 14407 | ≤41 |
| II | 150M | 75 | 10307 | 28477 | ≤3 |
| Total | \ | 174 | 17898 | 42884 | ≤44 |

FF: flip-flop, LUT: look-up table, RT: running time of program

**TABLE 2.** PL resource utilization and run time of local 2D entropy program.

| Step | Clock | DSP48E | FF | LUT | RT(ms) |
|---|---|---|---|---|---|
| I | 150M | 38 | 3628 | 6413 | ≤6 |
| II | 150M | 75 | 10307 | 28477 | ≤3 |
| Total | \ | 113 | 13935 | 34890 | ≤9 |

FF: flip-flop, LUT: look-up table, RT: running time of program

The calculation of 2D entropy or local 2D entropy is divided into the following steps. (I) The average gray value of the image is calculated in Formula (2). (II) The result is obtained according to Formula (1) or (3). The logic clock is 150M. The 2D entropy program requires only less than 44 ms, and the local 2D entropy program requires less than 9 ms. The second steps of 2D entropy and local 2D entropy program are identical. Thus, they are executed in the same PL module.

### C. IMAGE ACQUISITION WITH CLOSED-LOOP CONTROL

An IQA method is designed for acquiring satisfactory pattern images at high speeds. 2D entropy and local 2D entropy score the quality of captured images. The 2D entropy of an image increases with the level of illumination, whereas the 2D local entropy decreases. Thus, intervals of scores are set for both methods to represent good-quality images. We propose a closed-loop control of LED brightness that is based on the scores of the 2D entropy and the local 2D entropy assessment. The diagram of the LED illumination closed-loop control module is shown in Fig. 6. The PWM duty cycle starts with a relatively small value. The ROI image is extracted, and the local 2D entropy is evaluated only when the 2D entropy reaches its predefined threshold interval; these conditions promote system efficiency. The PWM duty cycle is adjusted until the scores from the 2D entropy assessment and the local 2D entropy assessment reach the threshold intervals. The PWM duty cycle then stops changing, and the images are saved for subsequent processing. The threshold intervals are determined by experiments.

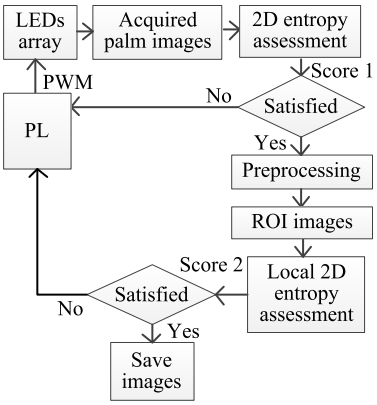


**FIGURE 6.** Diagram of LED illumination control module.

**TABLE 3.** Values of 2D image entropy and local 2D image entropy in Fig. 5.

| Sample | $H_{2D}$ | $H_{2D\_Local}$ |
|---|---|---|
| Fig. 5 (a) | 7.28 | 6.81 |
| Fig. 5 (b) | 8.73 | 6.61 |
| Fig. 5 (c) | 8.90 | 6.41 |
| Fig. 5 (d) | 9.96 | 5.05 |

$H_{2D}$: 2D image entropy, $H_{2D\_Local}$: local 2D image entropy

The 2D image entropy and local 2D image entropy values in Fig. 5 are listed in Table 3, where Fig. 5 (d) has the highest 2D entropy and the lowest local 2D entropy. The experimental results show that the 2D entropy between 8.8 and 9.2 and the local 2D entropy between 6.4 and 6.6 are the best threshold intervals for our proposed system in acquiring palm vein and palmprint images.

### D. IMAGE-LEVEL FUSION STRATEGY

Multimodal systems can achieve higher recognition rate than can one-modal systems, where feature fusion is required. Multimodal biometric feature fusion can be categorized into image-, feature-, score-, and decision-level fusion [42]. In the traditional palm vein processing method, the palmprint in the palm vein image is treated as noise that must be removed. In our experiment, the palmprint and palm vein images are captured simultaneously by the same camera, thereby preventing possible errors caused by calibration. In addition, the palmprint in palm vein images can be used as a criterion against which the quality of the fused image can be checked.

Different image-level fusion strategies have been proposed according to various requirements. Wavelet transform is used to gain the approximation coefficient matrices, where the image size is smaller than originate image matrices, because the embedded platform with limited resources should have less calculation and memory requirements. Then, the fused image is obtained by fusing these coefficient matrices. However, for the PC platform, we use complex wavelet transform to gain complex coefficient matrices and fuse them. Then, the fused image is obtained by using the inverse wavelet transform for fused coefficient matrices.

#### 1) IMAGE-LEVEL FUSION BASED ON WAVELET TRANSFORM

The proposed image-level fusion strategy for the embedded platform is as follows:

$$A_{xy} = \phi(\omega(\omega(f_1(x, y)), \omega(\omega(f_2(x, y))))), \tag{4}$$

where $\omega$ is a function used to gain the approximation coefficient matrices of the single-level discrete 2D wavelet decomposition, $\varphi$ is the fusion rule, and $f_1$ and $f_2$ are the images to be fused.

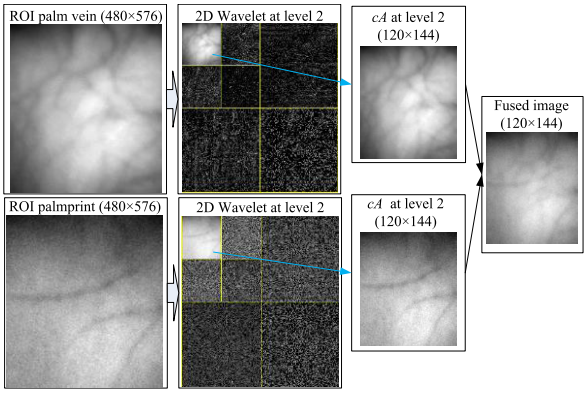


**FIGURE 7.** Image-level fusion strategy.

The image-level fusion strategy is shown in Fig. 7, where 2D wavelet at level 2 is applied in the ROI palm vein and palmprint images. In Fig. 7, *cA* represents the approximation coefficient matrix of the input image at level 2 of the wavelet, and the means of the *cA*s are then fused. The prototype system can capture palm vein and palmprint images with a resolution of 1200×1600. The ROI of palm images can be achieved with a resolution of 480×576 and then fused with a resolution of 120×144 at level 2 of the wavelet, as shown in Fig. 7. The ROI of palm images can also be fused with resolutions of 60×72, 30×36, and 15×18 at levels 3, 4, and 5, respectively. Close observation of Fig. 7 indicates that the fused images not only have palm vein but also palmprint features.

#### 2) IMAGE-LEVEL FUSION BASED ON COMPLEX WAVELET TRANSFORM

Complex wavelet transform is applied for image fusion on the PC platform. The complex wavelet is better than the wavelet because aliasing occurs when the wavelet transform is used for image fusion [43].

The fusion strategy is as follows:

$$f(x, y) = icw(\phi(c\omega(f_1(x, y)), c\omega(f_2(x, y)))), \tag{5}$$

where $c\omega$ denotes complex wavelet transform, $ic\omega$denotes inverse complex wavelet transform, and $\varphi$is the fusion function and described as follows:

$$LC_f(i, j) = (LC_p(i, j) + LC_v(i, j))/2, \tag{6}$$

$$HC_f^s(i,j) = \begin{cases} HC_p^s(i,j), & \text{mod}(HC_p^s(i,j)) \geq \text{mod}(HC_v^s(i,j)) \\ HC_v^s(i,j), & \text{mod}(HC_p^s(i,j)) < \text{mod}(HC_v^s(i,j)). \end{cases} \tag{7}$$

In the complex wavelet transform, the palm vein image and the palmprint image are decomposed into a complex low-pass coefficient matrix and a series of complex high-pass coefficient matrices, respectively [44]. $LC_T$ and $HC_T^s$ are used to denote the low-pass coefficient matrix and the high-pass coefficient matrices, respectively. Parameter $T$ can be $p$, $v$, or $f$, corresponding to palmprint image, palm vein image, and fused image, respectively. $s$=*{1,2…N},* where $N$ is the number of high-band coefficient matrices. *mod* is the function to calculate the module value of a complex number. In Equation (6), the fused low-pass coefficient matrix is the mean of two low-pass coefficient matrices, which are from the palmprint image and the palm vein image. In Equation (7), the comparative result of every pair of complex numbers at the same position from every pair of high-pass coefficient matrices shows that the complex number with module value is larger. The former fusion method can gain more low-frequency information, but the latter retains high-frequency details.

## IV. FEATURE EXTRACTION AND RECOGNITION ALGORITHMS

### A. FEATURE EXTRACTION BASED ON DEEP SCATTERING CONVOLUTIONAL NETWORK

Convolutional networks and deep learning algorithms are widely used in many object recognition problems [45]. The application of scattering transform for palm feature extraction is thus explored. DSCN provides a multilayer representation of the signal. Local descriptors of the input signal are computed with a cascade of three operations, namely, wavelet decomposition, complex modulus, and local averaging.

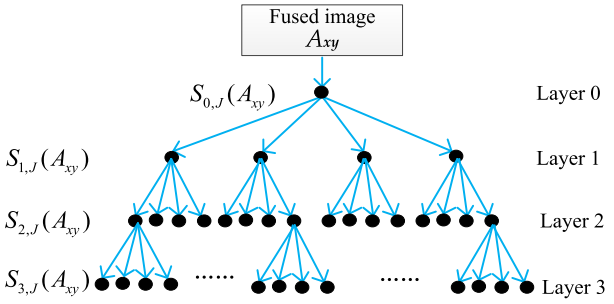


**FIGURE 8.** Deep scattering convolutional network.

An illustration of the DSCN is shown in Fig. 8, where the fused palm images are represented by matrices $Axy$. The first scattering coefficient is obtained as follows:

$$S_{0,J}(A_{xy}) = A_{xy} * \xi_J, \tag{8}$$

where $\xi_J$ is an averaging filter and $*$ denotes the spatial convolution. DSCN uses wavelet transforms at different scales and orientations, removes the complex phase, and calculates their average to obtain the scattering coefficient in the first layer by using the following equation:

$$S_{1,J}(A_{xy}) = \left|A_{xy} * \psi_{j_1,\lambda_1}\right| * \xi_J, \tag{9}$$

where $\Psi j_1, \lambda_1$ is a wavelet function, and $j_1$ and $\lambda_1$denote different scales and orientations, respectively. The second layer uses wavelets at scale $j_2$and orientations $\lambda_2$ in the following:

$$S_{2,J}(A_{xy}) = \left|\left|A_{xy} * \psi_{j_1,\lambda_1}\right| * \psi_{j_2,\lambda_2}\right| * \xi_J, \tag{10}$$

where $j2 < j1$. The third layer is as follows:

$$S_{3,J}(A_{xy}) = \left|\left|\left|A_{xy} * \psi_{j_1,\lambda_1}\right| * \psi_{j_2,\lambda_2}\right| * \psi_{j_3,\lambda_3}\right| * \xi_J, \tag{11}$$

where $j_3 < j_2 < j_1$. The third-layer scattering coefficients, and the mean and variance of these coefficients are calculated and used as features in SVM.

The dimension of the extracted feature is proportional to the number of DSCN parameters consisting of the scales and orientations in every layer. When the number of scales, the number of orientations or the depth of DSCN, is set bigger, the dimension of feature becomes higher. It can lead to better performance, but requires more run time for feature extraction and larger memory for feature storage. In this study, in order to reduce memory storage and computation time, three layers are implemented in DSCN.

### B. RECOGNITION ALGORITHM BASED ON SVM

SVM is a well-known machine learning approach designed for classification. In our implementation, the lib-SVM [46] toolbox version 3.21 is used for training and recognition. We select half of the samples for the training phase and leave the remaining samples for the test phase. For SVM training, the kernel function selected is the Gaussian radial basis function (RBF). The optimal penalty parameter C and the kernel coefficient Gamma are obtained from a set of parameters via the grid search function.

## V. DATABASE CREATION AND EXPERIMENTS

### A. DATABASE CREATION

A database consisting of palmprint and palm vein images is created using our self-designed system to evaluate the system performance. Images are obtained in a laboratory environment with temperatures from 20 °C to 25 °C and humidity of <90%. Twenty-seven persons participate in our experiment, and 10 palm vein images and 10 palmprint images of the right hand of each person are captured in different months. The raw image size is 1200×1600, the ROI size is 480×576, and the fused ROI images can be 120×144, 60×72, 30×36, and 15×18 at different wavelet levels. We obtain 540 ROI images from our LPVPPIS and 270 fused images in each type of resolution. For every person, half of the fused images are randomly selected for training, and the remaining images are used for recognition. The subjects simply position their hands freely above the prototype during data acquisition.

### B. EXPERIMENTS AND COMPARISONS

We conduct experiments on our own database and the PolyU multispectral palmprint database. The first fusion strategy (based on wavelet transform) is applied on our own database, and the second fusion method (based on complex wavelet transform) is applied on the PolyU database.

The hardware environment includes a Lenovo T430 laptop with Intel Core i5 (2.5 GHz) and 4 GB DDR3 SDRAM. The software environment comprises 32-bit Windows 7 and MATLAB (R2015a). The false accept rate (FAR) is the probability that the system inaccurately authorizes a non-authorized person because of inaccurately matching the biometric input with a template. The false reject rate (FRR) is the probability that the system inaccurately rejects the access request of an authorized person because of failure to match the biometric input with a template. The accuracy of biometric systems is expressed by its equal error rate (EER) when FAR and FRR are equal. The system performs better when the number is lower.

#### 1) EXPERIMENTS ON OUR OWN DATABASE

The results of our palm vein database alone, palmprint database alone, and fused database experiments using DSCN for feature extraction and SVM for training and recognition are listed in Table 4. Image databases of the same size of ROI are created, and the computation time required for each fusion strategy is measured for a further demonstration of computational efficiency. The average fusion time per image in our proposed fusion method is approximately 31 ms shorter than that in Wang's fusion strategy [20], and our technique achieves a much lower EER than databases of palm vein alone and palmprint alone. The result shows that LPVPPIS achieves an EER of 1.48%. As shown in Table 4, ROI images have 15×18 pixels. All the EERs drop to zero 60×72 if pixel or larger images are used.

**TABLE 4. Comparison of the palm vein, palmprint, and fused database experiments.**

| Database | Fusion strategy | $T_{fpi}$ | $P_{roi}$ | EER (%) |
|---|---|---|---|---|
| $D_{PV}$ | - | - | 15×18 | 1.85 |
| $D_{PP}$ | - | - | 15×18 | 2.22 |
| $D_{FD}$ | In [20] | 84 ms | 15×18 | 1.48 |
| $D_{FD}$ | Proposed | 53 ms | 15×18 | 1.48 |

$T_{fpi}$: fusion time per image
$P_{roi}$: pixel count of ROI images
$D_{PV}$: database of palm vein alone
$D_{PP}$: database of palmprint alone
$D_{FD}$: database of fused palm vein and palmprint

A comparative study of feature extraction algorithms (2DPCA, 2DFLD, 2DPCA plus 2DFLD, and proposed DSCN algorithms) is performed. The results listed in Table 5 show that the size of eigenvalue matrices in 2DPCA and 2DFLD are larger than those in the proposed method. The various EER curves are illustrated in Fig. 9. As shown in Table 5 and Fig. 9, the memory requirement for feature extraction is less when image ROI is small. Our proposed feature extraction algorithm requires much less memory for ROI images than 2DPCA and 2DFLD due to smaller ROI images, but it still achieves a lower EER.

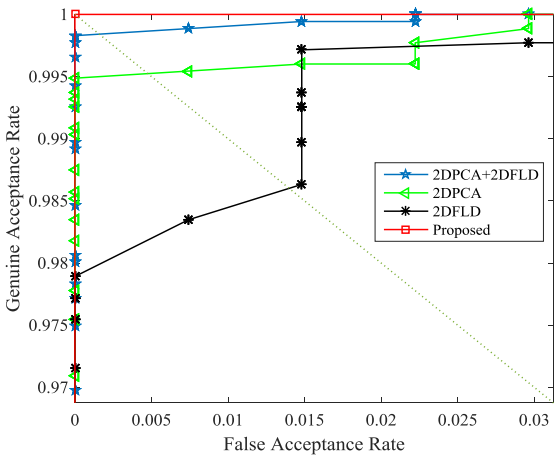


**FIGURE 9. Illustration of various EER curves.**

**TABLE 5. Comparison of fused database experiment results using different feature extraction algorithms.**

| Feature extraction | $P_{roi}$ | $S_{em}$ | EER (%) |
|---|---|---|---|
| 2DPCA [25] | 120×144 | 1200 | 0.49 |
| 2DFLD [26] | 120×144 | 1200 | 1.3 |
| 2DPCA+2DFLD [27] | 120×144 | 1200+100 | 0.23 |
| Proposed | 120×144 | 720 | 0 |
| Proposed | 60×72 | 720 | 0 |

$S_{em}$: size of eigenvalue matrix

#### 2) EXPERIMENTS ON POLYU DATABASE

The PolyU multispectral palmprint database is composed of 3000 images from 250 individuals with 12 images from each individual. Samples were collected in two separate sessions with six images in one session, and the average time interval between two sessions was approximately nine days [47]. We select images collected by NIR illumination as palm vein images and images collected by blue illumination as palmprint images. Complex wavelet transform is used for image fusion.

ROI images with a resolution of 128x128 provided in the PolyU multispectral palmprint database are used for experiments. Images from the first session are used for training and the remaining images for testing. PCA is applied on the extracted features to reduce their dimensionality and thus improve algorithm efficiency. Feature dimensionality is reduced to 100 after PCA, and sign 8-bit number is used to store features by retaining the integer part of the PCA result. A comparison of recognition accuracy and template size is shown in Table 6. The template size is the average size required for storing the coefficients for a single training image.

**TABLE 6. Comparison of recognition rate and template size.**

| Method | Recognition rate | TS (in bytes) |
|---|---|---|
| NMRT [12] | 100% | 486 |
| Hessian Phase [12] | 99.63% | 2592 |
| Ordinal Code [19] | 99.93% | 7776 |
| Laplacian Palm [20] | 82.73% | 22384 |
| Comp Code [3] | 98.97% | 7776 |
| Proposed | 99.97% | 100 |

TS: template size

As shown in Table 6, Comp Code and Ordinal Code have the same template size, which is much smaller than Laplacian Palm, and they achieve a higher recognition rate than Laplacian Palm. Hessian Phase has smaller template size than these methods, but its recognition rate is lower than that of Ordinal Code. The proposed method and NMRT outperform the other methods, but the proposed method has the least template size, which is almost a fifth of that of NMRT, with only a 0.03% decrease in recognition rate. The proposed method can generally achieve a comparatively higher recognition rate, but it has the least storage memory for training images.

## VI. DISCUSSIONS

### A. VISUAL SENSOR

The visual sensor for the vision-based personal identification system (VBPIS) can be an NIR-sensitive camera [13], a regular CMOS, or a high-resolution charge-coupled device (CCD) [3], [4], [20] camera. A key contributing factor for accurate measurements is the calibration of the camera position and exposure, regardless of the type of visual sensor. This study focuses on designing an LPVPPIS and introduces a CMOS visual sensor in the proposed system because it is usually less costly than some CCD visual sensors. In our proposed system, a capture cycle (including palm vein and palmprint) can be completed within 1 or 2 s. The position of the camera is almost fixed, and the exposure can be adjusted according to our proposed IQA method.

### B. OPERATION UNIT

The operation unit receives the image acquired by the visual sensor and performs the necessary operations to obtain the desired measurements. This unit can be implemented on a general-purpose computer [3], [4], [20] or dedicated hardware [13]. A SoC is introduced in the LPVPPIS because it integrates the merit of ARM cortex-A9 and FPGA, which reduces the size of PCB compared with the ARM-alone or FPGA-alone system.

### C. IQA METHOD

The accuracy of the VBPIS is usually influenced by the raw image quality, especially the effect of various lighting conditions. The low quality of the sensor image seriously affects the system performance. Palm vein recognition technology is not as mature as fingerprint or iris technology, especially in image acquisition. Betta *et al*. [7] defined suitable reference conditions for face image acquisition (in terms of luminance, acquisition settings, system defocus, and motion blur), which corresponds to related reference values for the quantities of influence. The palm image acquisition system based on IQA must consider the characteristics of lighting conditions. However, given that the real-time IQA method is rarely discussed in VBPIS, we provide one solution.

### D. FUSION STRATEGY

We propose two different fusion strategies for different requirements.

When the wavelet transform method is adopted, the processing complexity is high and the information describing the input pattern is rich when the fusion level is low. Wavelet transform can hierarchically decompose a signal into low- and high-frequency components, providing a multiresolution analysis of the signal. Hosseini *et al*. [4] extracted invariant features from VL and NIR iris images, whose fusion led to higher classification accuracy. Some image-level fusion methods were also introduced [20]. In the present study, we use more than two levels of approximation coefficients of wavelet into one single image. The advantages of using more than two levels compared with only one level of approximation coefficients include less storage requirement and less image processing operations.

The complex wavelet method is proposed without considering the resources. Thus, the fused image has the same size as the original image. The fusion strategy can gain more low-frequency information from two images while maintaining high-frequency details.

## VII. CONCLUSION

We propose a biometric pattern acquisition system called LPVPPIS, and the total cost of the system components is less than US$100. An IQA method based on 2D entropy and local 2D entropy is proposed for acquiring the palm images to remarkably improve the image quality. We use an image-level fusion strategy that is based on approximation coefficients of wavelet for palm vein and palmprint biometric features. Another image-level fusion strategy based on complex wavelet is proposed for different requirement. Finally, we apply DSCN for feature extraction and SVM for training and recognition. Our experiments on our own database prove that the proposed fusion strategy and feature extraction algorithm in our LPVPPIS achieves substantially less operational requirement than the previous fusion strategy. It has less memory requirement and lower EER than the 2DPCA and 2DFLD feature extraction algorithms. In addition, experiments on the PolyU database validate the robustness of our method. Thus, we conclude that LPVPPIS can be used in daily life.

## REFERENCES

[1] A. K. Jain, A. Ross, and S. Prabhakar, "An introduction to biometric recognition," *IEEE Trans. Circuits Syst. Video Technol.*, vol. 14, no. 1, pp. 4–20, Jan. 2004.

[2] K. C. Chan, Y. S. Moon, and P. S. Cheng, "Fast fingerprint verification using subregions of fingerprint images," *IEEE Trans. Circuits Syst. Video Technol.*, vol. 14, no. 1, pp. 95–101, Jan. 2004.

[3] D. Zhang, Z. Guo, G. Lu, L. Zhang, and W. Zuo, "An online system of multispectral palmprint verification," *IEEE Trans. Instrum. Meas.*, vol. 59, no. 2, pp. 480–490, Feb. 2010.
[4] M. S. Hosseini, B. N. Araabi, and H. Soltanian-Zadeh, "Pigment melanin: Pattern for iris recognition," *IEEE Trans. Instrum. Meas.*, vol. 59, no. 4, pp. 792–804, Apr. 2010.
[5] J. Daugman, "How iris recognition works," *IEEE Trans. Circuits Syst. Video Technol.*, vol. 14, no. 1, pp. 21–30, Jan. 2004.
[6] H. Hu, "Sparse discriminative multimanifold Grassmannian analysis for face recognition with image sets," *IEEE Trans. Circuits Syst. Video Technol.*, vol. 25, no. 10, pp. 1599–1611, Oct. 2015.
[7] G. Betta, D. Capriglione, M. Corvino, C. Liguori, and A. Paolillo, "Face based recognition algorithms: A first step toward a metrological characterization," *IEEE Trans. Instrum. Meas.*, vol. 62, no. 5, pp. 1008–1016, May 2013.
[8] P. MacGregor and R. Welford, "Veincheck: Imaging for security and personnel identification," *Adv. Imag.*, vol. 6, no. 7, pp. 52–56, 1991.
[9] D. Zhang, W.-K. Kong, J. You, and M. Wong, "Online palmprint identification," *IEEE Trans. Pattern Anal. Mach. Intell.*, vol. 25, no. 9, pp. 1041–1050, Sep. 2003.
[10] A. Kong, D. Zhang, and M. Kamel, "A survey of palmprint recognition," *Pattern Recognit.*, vol. 42, no. 7, pp. 1408–1418, Jul. 2009.
[11] W. Kang and Q. Wu, "Contactless palm vein recognition using a mutual foreground-based local binary pattern," *IEEE Trans. Inf. Forensics Security*, vol. 9, no. 11, pp. 1974–1985, Nov. 2014.
[12] Y. Zhou and A. Kumar, "Human identification using palm-vein images," *IEEE Trans. Inf. Forensics Security*, vol. 6, no. 4, pp. 1259–1274, Dec. 2011.
[13] S. Joardar, A. Chatterjee, and A. Rakshit, "A real-time palm dorsa subcutaneous vein pattern recognition system using collaborative representation-based classification," *IEEE Trans. Instrum. Meas.*, vol. 64, no. 4, pp. 959–966, Apr. 2015.
[14] H. C. Lee, B. J. Kang, E. C. Lee, and K. R. Park, "Finger vein recognition using weighted local binary pattern code based on a support vector machine," *J. Zhejiang Univ. Sci. C*, vol. 11, no. 7, pp. 514–524, Jul. 2010.
[15] J. E. S. Pascual, J. Uriarte-Antonio, R. Sanchez-Reillo, and M. G. Lorenz, "Capturing hand or wrist vein images for biometric authentication using low-cost devices," in *Proc. 6th Int. Conf. Intell. Inf. Hiding Multimedia Signal Process.*, Oct. 2010, pp. 318–322.
[16] H. Zhang, C. Tang, A. W.-K. Kong, and N. Craft, "Matching vein patterns from color images for forensic investigation," in *Proc. IEEE 5th Int. Conf. Biometrics, Theory, Appl., Syst.*, Sep. 2012, pp. 77–84.
[17] Y. Lin, E. Y. Du, Z. Zhou, and N. L. Thomas, "An efficient parallel approach for sclera vein recognition," *IEEE Trans. Inf. Forensics Security*, vol. 9, no. 2, pp. 147–157, Feb. 2014.
[18] L. Mirmohamadsadeghi and A. Drygajlo, "Palm vein recognition with local texture patterns," *IET Biometrics*, vol. 3, no. 4, pp. 198–206, Dec. 2014.
[19] Y. Hao, Z. Sun, T. Tan, and C. Ren, "Multispectral palm image fusion for accurate contact-free palmprint recognition," in *Proc. Int. Conf. Image Process.*, Oct. 2008, pp. 281–284.
[20] J.-G. Wang, W.-Y. Yau, A. Suwandy, and E. Sung, "Fusion of palmprint and palm vein images for person recognition based on 'Laplacianpalm' feature," in *Proc. Comput. Vis. Pattern Recognit.*, Jun. 2007, pp. 1–8.
[21] Y. H. Lee, M. Khalil-Hani, and R. Bakhteri, "FPGA-based finger vein biometric system with adaptive illumination for better image acquisition," in *Proc. IEEE Symp. Comput. Appl. Ind. Electron.*, Dec. 2012, pp. 107–112.
[22] S. Crisan, I. G. Tarnovan, and T. E. Crisan, "Radiation optimization and image processing algorithms in the identification of hand vein patterns," *Comput. Standards Interfaces*, vol. 32, no. 3, pp. 130–140, Mar. 2010.
[23] J.-C. Lee, "A novel biometric system based on palm vein image," *Pattern Recognit. Lett.*, vol. 33, no. 12, pp. 1520–1528, Sep. 2012.
[24] L. Wang, G. Leedham, and D. Siu, "Minutiae feature analysis for infrared hand vein pattern biometrics," *Pattern Recognit.*, vol. 41, no. 3, pp. 920–929, Mar. 2008.
[25] J. Yang, D. Zhang, A. F. Frangi, and J.-Y. Yang, "Two-dimensional PCA: A new approach to appearance-based face representation and recognition," *IEEE Trans. Pattern Anal. Mach. Intell.*, vol. 26, no. 1, pp. 131–137, Jan. 2004.
[26] H. Xiong, M. N. S. Swamy, and M. O. Ahmad, "Two-dimensional FLD for face recognition," *Pattern Recognit.*, vol. 38, no. 7, pp. 1121–1124, Jul. 2005.
[27] R. M. Mutelo, L. C. Khor, W. L. Woo, and S. S. Dlay, "A novel Fisher discriminant for biometrics recognition: 2DPCA plus 2DFLD," in *Proc. IEEE Symp. Circuits Syst.*, May 2006, pp. 4325–4328.
[28] Y. LeCun, Y. Bengio, and G. Hinton, "Deep learning," *Nature*, vol. 521, pp. 436–444, May 2015.
[29] A. Krizhevsky, I. Sutskever, and G. E. Hinton, "ImageNet classification with deep convolutional neural networks," in *Proc. Neural Inf. Process. Syst.*, 2012, pp. 1090–1098.
[30] G. Hinton *et al.*, "Deep neural networks for acoustic modeling in speech recognition: The shared views of four research groups," *IEEE Signal Process. Mag.*, vol. 29, no. 6, pp. 82–97, Nov. 2012.
[31] J. Bruna and S. Mallat, "Classification with scattering operators," in *Proc. IEEE Conf. Comput. Vis. Pattern Recognit.*, Jun. 2011, pp. 1561–1566.
[32] J. Bruna and S. Mallat, "Invariant scattering convolution networks," *IEEE Trans. Pattern Anal. Mach. Intell.*, vol. 35, no. 8, pp. 1872–1886, Aug. 2013.
[33] S. Minaee and Y. Wang, "Fingerprint recognition using translation invariant scattering network," in *Proc. IEEE Signal Process. Med. Biol. Symp. (SPMB)*, Philadelphia, PA, USA, Dec. 2015, pp. 1–6.
[34] *Lynx-2048-GigE*. Accessed: Oct. 18, 2016. [Online]. Available: http://www.xenics.com/en/camera/lynx-2048-gige
[35] *GL2048R*. Accessed: Oct. 18, 2016. [Online]. Available: http://www.sensorsinc.com/products/detail/gl2048-r-ingaas-linescan-camera
[36] Xilinx, Inc. *Zynq-7000 All Programmable SoC Overview, Datasheet*. Accessed: Oct. 18, 2015. [Online]. Available: http://www.xilinx.com/support/documenta-tion/data_sheets/ds190-Zynq-7000-Overview.pdf
[37] J.-G. Wang, W.-Y. Yau, A. Suwandy, and E. Sung, "Person recognition by fusing palmprint and palm vein images based on 'Laplacianpalm' representation," *Pattern Recognit.*, vol. 41, no. 5, pp. 1514–1527, 2008.
[38] OmniVision Technologies, Inc. *OV2640: 2 MPixel Product Brief, Datasheet*. Accessed: Oct. 18, 2015. [Online]. Available: http://www.ovt.com/up-loads/parts/OV2640_PB(2.4).pdf
[39] Monolithic Power System, Inc. *MP3202: 1.3 A Fixed Frequency White LED Driver, Datasheet*. Accessed: Oct. 18, 2015. [Online]. Available: http://www.monolith-icpower.com
[40] N. Otsu, "A threshold selection method from gray-level histograms," *IEEE Trans. Syst., Man, Cybern.*, vol. SMC-9, no. 1, pp. 62–66, Jan. 1979.
[41] M. Shahid, A. Rossholm, B. Lövström, and H.-J. Zepernick, "No-reference image and video quality assessment: A classification and review of recent approaches," *EURASIP J. Image Video Process.*, vol. 2014, no.1, pp. 1, Dec. 2014.
[42] A. Ross and A. Jain, "Information fusion in biometrics," *Pattern Recognit. Lett.*, vol. 24, no. 13, pp. 2115–2125, 2003.
[43] H. R. Shahdoosti and A. Mehrabi, "MRI and PET image fusion using structure tensor and dual ripplet-II transform," *Multimedia Tools Appl.*, vol. 77, pp. 22649–22670, Aug. 2017, doi: 10.1007/s11042-017-5067-1.
[44] S. M. Hazavei and H. R. Shahdoosti. (2017). "Using complex wavelet transform and bilateral filtering for image denoising." [Online]. Available: https://arxiv.org/abs/1702.01276
[45] A. Voulodimos, N. Doulamis, A. Doulamis, and E. Protopapadakis, "Deep learning for computer vision: A brief review," *Comput. Intell. Neurosci.*, vol. 2018, Feb. 2018, Art. no. 7068349, doi: 10.1155/2018/7068349.
[46] *Libsvm*. Accessed: Oct. 18, 2016. [Online]. Available: http://www.csie.ntu.edu.tw/~cjlin/libsvm
[47] *PolyU Multispectral Palmprint Database*. Accessed: Apr. 25, 2018. [Online]. Available: http://www4.comp.polyu.edu.hk/~biometrics/

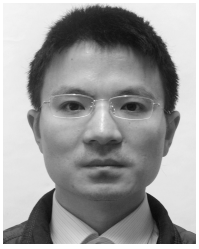

**PENG CHEN** was born in Zhejiang, China, in 1981. He received the B.Sc. and Ph.D. degrees from Zhejiang University, Hangzhou, China, in 2003 and 2009, respectively. He was a Visiting Scholar with the University of California at Santa Barbara, Santa Barbara, CA, USA, from 2015 to 2016. He is currently an Associate Professor with the Zhejiang University of Technology. His research interests include computer vision and signal processing.

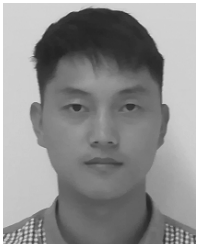

**BAOJIN DING** was born in Anhui, China, in 1994. He received the B.Sc. degree from the Faculty of Mechanical Engineering and Automation, Zhejiang Sci-Tech University, Hangzhou, China, in 2015. He is currently pursuing the Ph.D. degree in control science and engineering with the Zhejiang University of Technology. His current research interests include biometric pattern recognition and field-programmable gate array-based signal processing.

**HAIXIA WANG** received the B.S. and Ph.D. degrees in computer engineering from Nanyang Technological University, Singapore, in 2007 and 2012, respectively. She is currently an Associate Professor with the College of Information Engineering, Zhejiang University of Technology, China. Her research interests include image inpainting, fringe pattern processing, and 3D shape measurements.

**RONGHUA LIANG** received the B.S. degree from Hangdian University, in 1996, and the Ph.D. degree in computer science from Zhejiang University, in 2003. He was a Research Fellow with the University of Bedfordshire, U.K., from 2004 to 2005, and a Visiting Scholar with the University of California at Davis, Davis, CA, USA, from 2010 to 2011. He is currently a Professor with the College of Information Engineering, Zhejiang University of Technology, China. His research interests include computer vision, computer graphics, and medical visualization. He is a Senior Member of the IEEE.

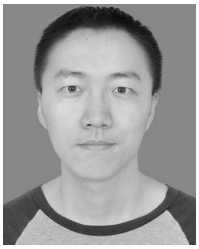

**YILONG ZHANG** was born in Shaanxi, China, in 1988. He received the Ph.D. degrees in physics from Tsinghua University, Beijing, China, in 2017. He currently holds a Postdoctoral position at the College of Information Engineering, Zhejiang University of Technology. His research interests include biomedical optical imaging and optical biosensing.

**WEI ZHU** was born in Zhejiang, China, in 1982. He received the B.Sc. and Ph.D. degrees from Zhejiang University, Hangzhou, China, in 2004 and 2010, respectively. He is currently an Associate Professor with the Zhejiang University of Technology. His research interests include signal processing and video coding.

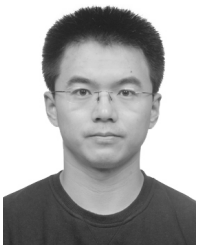

**YIPENG LIU** received the Ph.D. degree in control science and engineering from the Harbin Institute of Technology, China, in 2015. He was a Visiting International Student in medical physics with The University of Chicago, USA, from 2012 to 2013. He is currently an Assistant Professor of pattern recognition and intelligent system with the Zhejiang University of Technology, China. His research interests include computational modeling and machine learning in medical image analysis, with an emphasis on brain connectivity and eye fundus image analysis.